RSC Advances

ROYAL SOCIETY OF CHEMISTRY

www.rsc.org/advances

Journal Name

ARTICLE

Boron and phosphorous-doped graphene as metal-free electrocatalyst for oxygen reduction reaction in alkaline medium

Received 00th January 20xx,
Accepted 00th January 20xx

DOI: 10.1039/x0xx00000x

www.rsc.org/

Gayoung Jo, Jakkid Sanetuntikul and Sangaraju Shanmugam*

An efficient solid-state pyrolysis route is presented to prepare boron and phosphorous-doped graphene without using the template, solvent, or catalyst. By controlling the pyrolysis temperature, selective doping of phosphorous or boron was achieved. Phosphorous-doped graphene (PDG) and boron-doped graphene (BDG) samples are obtained when pyrolysing the precursor at 700 ˚C and at 900 ˚C, respectively under autogenic pressure. PDG and BDG electrodes show a considerable oxygen reduction activity by direct four-electron pathway in alkaline medium. Further, these catalysts show improved durability under continuous oxygen reduction, resistance to methanol oxidation and CO-tolerance than the commercial catalyst. The results suggest that by tuning the reaction temperature, selective doping, and either boron or phosphorous in graphene was achieved and used as non-precious and metal-free catalysts for oxygen reduction.

1. Introduction

Fuel cell electrodes account for 33% of the whole cost of fuel cells[1] because the use of precious platinum in both electrodes. Therefore, the development of non-precious catalysts received tremendous importance in recent years to reduce the overall cost of the fuel cell electrode components.[2] An alkaline polymer electrolyte membrane fuel cell (APEFC) is a counterpart of PEMFC that uses an anionic exchange membrane. It allows the use of non-precious catalysts owing to its faster ORR kinetics and better stability of electrode materials under alkaline conditions.[3] For these reasons, we focus on the development of non-precious catalysts for the ORR in alkaline medium. Recently, heteroatom-doped carbon nanostructures have received enormous importance as non-precious-metal electrode materials for oxygen reduction.[4–9] Doping the heteroatom into a carbon network can be mainly conducted by (1) intercalation and (2) substitution.[10] Particularly, substitutional doping of heteroatom into carbon is able to modify the electronic properties of the carbon network, and accordingly tune the electrocatalytic activities.

Generally, three methods have been mainly reported to substitute heteroatom into the carbon network: (1) arc-discharge method,[11–13] (2) laser-ablation method,[14,15] and (3) chemical vapor deposition (CVD).[16,17] These techniques require high energy consumption, expensive hardware and multistep processes, which cause a costly manufacturing process. On the other hand, solid-state pyrolysis[7,9,18] is a cost-effective and facile single-step synthetic approach to fabricate heteroatom-doped carbon. The synthetic approach has been considered as a green process since the approach does not need templates, solvents, or catalysts. In addition, this process can be easily up-scaled.

Boron doping into a carbon network makes the host carbon array to have p-type conductivity and act as electron acceptor due to the strong electron withdrawing capability at the hexagonal site.[19–21] The strong electron withdrawing capability of doped-boron induces adsorption of O_2 molecular on the doped boron sites. Yang and coworkers[7] also illustrated that O_2 adsorption is favourable on boron dopant rather than adjacent carbon atoms by more positive charged boron atom than carbon atom[22,23] due to lower electronegativity of boron (2.0) than that of carbon atom (2.5). O_2 adsorption is important step for further steps for the oxygen reduction.[24] Whereas, phosphorous-doping, creates more positive charge than the parent carbon atom.[4] It indicates that O_2 adsorption is favourable on phosphorous atom in phosphorous doped-carbon, which is same tendency as doped boron atom into the carbon network. This tendency is due to lower electronegativity of phosphorous (2.1) than that of carbon (2.5) even though electron configuration and number of valence electron of phosphorous is same as nitrogen atom.

Even though, nitrogen-doped carbons have been widely investigated as oxygen reduction catalysts[6,7,18] a few reports emphasized phosphorous or boron-doped carbon as non-precious catalysts for ORR in alkaline medium. Herein, we describe a versatile and efficient synthetic route to dope heteroatom selectively using a single precursor. This method is facile, solvent-, catalyst-, and template-free and it is easy to handle, and thus might even be scalable. The prepared boron-doped graphene (BDG) or phosphorous-doped graphene (PDG) used as a metal-free electrocatalyst for the oxygen reduction

[a] Department of Energy Systems Engineering, Daegu Gyeongbuk Institute of Science and Technology (DGIST), Daegu, 711-873, Republic of Korea. E-mail: sangarajus@dgist.ac.kr ; Fax: (+82) 53 785 6409.

† Footnotes relating to the title and/or authors should appear here.
Electronic Supplementary Information (ESI) available: additional results. See DOI: 10.1039/x0xx00000x

reaction in alkaline electrolyte and these electrodes exhibited an efficient four-electron transfer process with high selectivity compared with a commercial Pt/C catalyst

2. Experimental

2.1 Preparation of BPG precursor

The graphene (N002-PDR, Angstrom materials) dispersion and tetraphenylphosphonium tetraphenylborate (TPP-TPB, Aldrich) solution were prepared separately with sonication of contents for 30 min. The graphene dispersion consists of 100 mg of graphene and 10 mL of ethanol, and the TPP-TPB solution consists of 200 mg of TPP-TPB and 10 mL of ethanol. The TPP-TPB (precursor) solution was slowly added into the graphene dispersion with magnetic stirring and heating at a temperature of 60 °C. Once the addition of TPP-TPB solution was finished, the temperature was kept for 6 h with continuous stirring. After 6 h, ethanol was removed by centrifugal separation, and dried at 60 °C under vacuum. Afterwards, B and P precursor impregnated graphene (BPG) was obtained, which was used as a precursor for the preparation of phosphorous-doped and boron-doped graphene as described in section 2.2.

2.2 Preparation of phosphorous-doped and boron-doped graphene

For a typical synthesis, 0.035 g of the BPG precursor was enclosed in a Swagelok union cell; subsequently it was thermally decomposed at a temperature of 700 °C and 900 °C for a period of 3 h in a tubular furnace under autogenic atmosphere without any gas flow. The cell was cooled automatically under ambient conditions. BPG precursor calcined at 700 °C and 900 °C was named as PDG and BDG, respectively. The kind of heteroatom that is doped into the graphene was determined by elemental composition analysis using XPS and ICP-MS. For purification, as-prepared PDG and BDG were treated with 10 mL of concentrated HCl (~37%) for 24 h to remove any oxide on the surface of the as-prepared samples. Acid treated samples were washed by using copious distilled water and ethanol, and dried overnight in a vacuum oven at 60 °C. All supernatant such as used HCl, distilled water, and ethanol were removed by using centrifugal separation at a rotation speed of 10,000 rpm for 10 min.

2.3 Physico-chemical characterization

Electron microscope studies were conducted to confirm the morphology and *d*-spacing (interlayer distance) using FE-TEM (Hitachi, HF-3300). Samples for the TEM studies were prepared by dropping ultrasonically dispersed solution of black powdered catalysts and isopropyl alcohol (IPA) on a substrate. As the substrate, copper (Cu) grid coated with amorphous carbon film was used for TEM measurements. TEM experiments were performed at an acceleration voltage of 300 kV. Crystallinity of products was studied by powder XRD (Panalytical, Empyrean) using Cu K-alpha radiation at a generator voltage of 40 kV and a tube current of 30 mA. To examine the nature of carbon with a ratio of structural defects to graphitic array, Raman spectroscopy was obtained by high resolution dispersive Raman microscope (Horiba Jobin Yvon, LabRAM HR UV/Vis/NIR). Elemental analysis was performed by XPS (Thermo Fisher Scientific, ESCALAB250 XPS system, Theta Probe XPS system) using monochromated Al K-alpha source at 15 kV and 150 W. Binding energy values at the x-axis were calibrated by using C1s from a carbon value taken as 284.6 eV. The amount of P and B contents in PDG and BDG catalysts were also analyzed by inductively coupled plasma-atomic emission spectroscopy (ICP-MS, Thermo Scientific, ICAP Q).

2.4 Electrochemical characterization

The ORR electrocatalytic performance of PDG and BDG catalysts was studied by cyclic voltammetry (CV) and linear sweep voltammetry (LSV) with a 3-electrode system using a bipotentiostat (Bio-Logic, VSP). For the 3-electrode system, a saturated calomel electrode (SCE, Hg/HgCl), a spiral platinum wire, and a glassy carbon electrode (GCE, Ø = 3 mm) were used as a reference, counter, and working electrode, respectively. The voltammograms were recorded in N_2- and O_2-saturated 0.1 M KOH aqueous solution at a scan rate of 10 mVs^{-1}. The N_2- and O_2-saturated electrolytes were prepared by bubbling N_2 and O_2 gas for 30 min at a flow rate of 80 sccm, respectively. For the working electrode, bare glassy carbon stuck in Teflon was used. On the bare glassy carbon electrode (GCE), catalyst ink was dropped on the surface, and dried at 50 °C in a forced convection oven; afterwards, Nafion® 5 wt% solution (Aldrich) was dropped on the top of dried catalyst ink. Nafion® was used as binder to hold the catalyst to the GCE. All the electrochemical experiments (CVs and LSVs) were continued until a stable voltammogram was obtained. Potential values were converted from saturated calomel electrode (SCE) to reversible hydrogen electrode (RHE), and current was normalized to the geometric area of electrode. For comparison, 10 wt% loaded Platinum on carbon black, Vulcan XC-72, (E-TEK) was used as a reference catalyst.

2.5 Catalyst ink preparation

The catalyst ink was prepared with 1 mg of black powdered PDG and BDG, and 100 µL of aqueous solution (distilled water: 75 µL, Nafion® 5 wt% solution: 20 µL, IPA: 5 µL). The ink was vigorously sonicated for 30 min using a sonicator. For CV, the working electrode was prepared by dropping 10 µL of catalyst ink on the surface of the glassy carbon electrode at first, and then 5 µL of Nafion® 5 wt% solution (Aldrich) was dropped on the same area. The ink coated GCE was dried at room temperature. For LSV, 5 µL of catalyst ink was dropped firstly, and then 2 µL of Nafion® 5 wt% solution (Aldrich) was dropped on the GCE.

2.6 Selectivity test: methanol oxidation and CO poisoning tolerance test

LSV technique was used with RDE technique and 3-electrode system for both methanol oxidation tolerance and CO poisoning effect tests. Methanol oxidation tolerance and CO poisoning tests were conducted at a potential window of 0.2 V to -0.8 V at a scan rate of 10 mVs^{-1} with the electrode rotation speed of 1600 rpm. O_2-saturated 0.1 M KOH was used as electrolyte. The experiments were conducted under two different environments. The first LSV was obtained in O_2-

saturated electrolyte. Afterwards, the second LSV was obtained in 2 mL of 2 M methanol added O_2-saturated electrolyte. To consider the sufficient mixing of methanol in electrolyte, the experiment started 10 min after the addition of methanol. O_2 bubbling was kept at a flow rate of 20 sccm during the experiments. CO poisoning effect test was investigated under three different environments. The first LSV was obtained in O_2-saturated 0.1 M KOH electrolyte. The second LSV was obtained in both CO and O_2-saturated electrolyte. To consider decreased partial pressure effect of O_2 gas in electrolyte due to addition of CO gas, the third LSV was obtained in both N_2- and O_2-saturated electrolyte. During the experiments, all gases bubbling (O_2, CO, and N_2) were kept at a flow rate of 20 sccm.

2.7 Durability test

A durability test under continuous oxygen reduction was conducted by chronoamperometric technique using the RDE technique at a fixed potential of -0.26 V vs. SCE for 43200 s (12 h) with an electrode rotation speed of 1600 rpm. A 3-electrode system was used with the same reference, counter, and working electrode as the previous electrochemical study. For electrolyte, O_2-saturated 0.1 M KOH aqueous solution was prepared by O_2-bubbling at a flow rate of 80 sccm for 30 min. During the experiments, O_2 gas bubbling was maintained at 20 sccm. The data was recorded every 100 μA and 5 s.

3. Results and discussion

Morphological studies using TEM revealed the thin sheet-like structures with random wrinkles of PDG and BDG (Fig. 1a and c), which is the same morphology as pristine graphene (Fig. S1, Supporting Information). High resolution TEM images show the presence of lattice fringes, which corresponding to the C(002) interlayer planar of carbon (Fig. 1b and d).

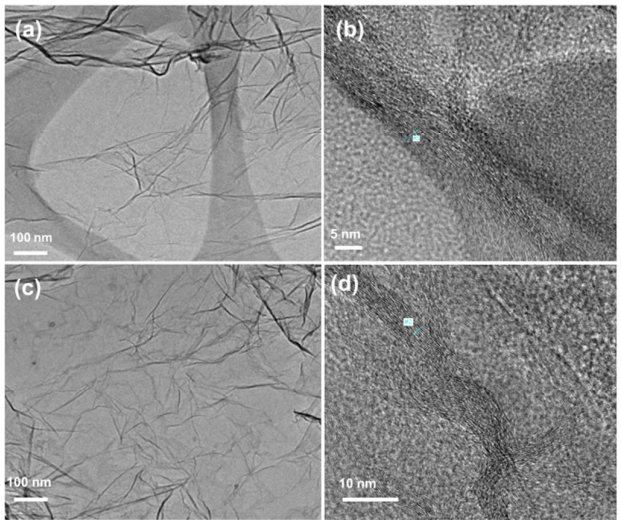

Fig. 1. Low resolution TEM images of (a) PDG and (c) BDG, High resolution TEM images of (b) PDG and (d) BDG with lattice fringes.

The interlayer distance obtained from the XRD results are 0.366, 0.353 and 0.369 nm for PDG, BDG and pristine graphene, respectively (Fig. 2). From the XRD data, the interlayer distances of PDG and BDG samples were found to be smaller than a pristine graphene. This change is due to heat treatment effect under high temperature, 700 °C and 900 °C. Takai et al.[24] and Endo et al.[25] reported that high temperature treatment decreases in the interlayer spacing. In fact, the interlayer distance of BDG (0.353 nm) is smaller than PDG (0.366 nm) owing to higher temperature treatment. Another evidence for higher interlayer distance of PDG is bigger covalent radius of phosphorous (110 pm) in PDG than boron (88 pm) doped in BDG.

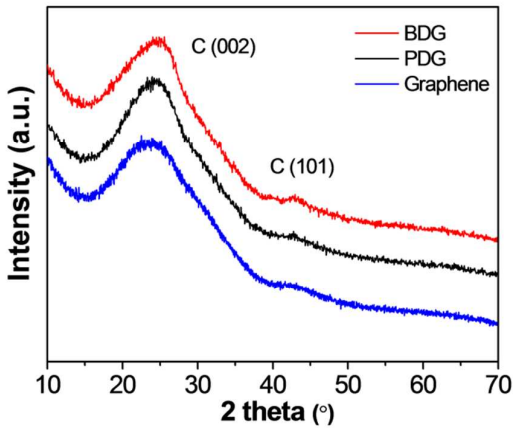

Fig. 2. XRD patterns of PDG, BDG, and pristine graphene.

The Raman spectra shown in Figure 3a exhibit the presence of two strong peaks at 1341 cm^{-1}, 1584 cm^{-1} for PDG and 1343 cm^{-1}, 1578 cm^{-1} for BDG. The bands observed at around 1341 cm^{-1}, and 1584 cm^{-1} correspond to D and G bands of carbon, respectively. The I_D/I_G ratio for PDG and BDG is 1.03 and 1.36, respectively, which indicates that BDG has more defects composition than PDG. The I_D/I_G ratio is 0.97 for pristine graphene sample. This observed difference in ratio can be attributed to the higher doping of heteroatom content in BDG than PDG. Generally, phosphorous[4,26] or boron[8,21,27–31] doping forms defect sites into the parent carbon network due to larger covalent radius of phosphorous and boron than carbon. More defect sites of BDG can contribute to providing more reaction sites for the oxygen reduction. This contribution can be proof of the higher ORR performance of BDG over PDG, which will be discussed further.

The wide XPS survey spectra show the presence of C, O, P, or B in PDG and BDG (Fig. 3b). Importantly, sample prepared at 700 °C exhibits only phosphorous (0.18 at.%), no boron was observed whereas the sample prepared at 900 °C possess only boron with a doping of 0.82 at.%, and surprisingly no phosphorous was observed (Table S1, Supporting Information). Further, the B & P contents present in the two catalysts were determined by ICP-MS analysis. The amount B & P contents were found to be 0.02 and 0.21 % for PDG and 0.91 and 0.04% for BDG sample, respectively. With

increase in the temperature of 200 °C that is from 700 to 900 °C, the doping of only boron in graphene was observed, suggesting that at 900 °C, phosphorous doping was not occurred, which may be due to the easy sublimation of elemental phosphorous compared with boron. Moreover, the higher doping concentration of B in BDG sample, indicates the easier doping of boron due to the similar covalent radius of boron with carbon atom rather than the doping of phosphorous into the carbon network. We observed that P and B doping levels decreased with increasing the temperature from 700 to 900 °C, this indicates that the heteroatom-doping level is non-linearly dependent on the heating temperature.

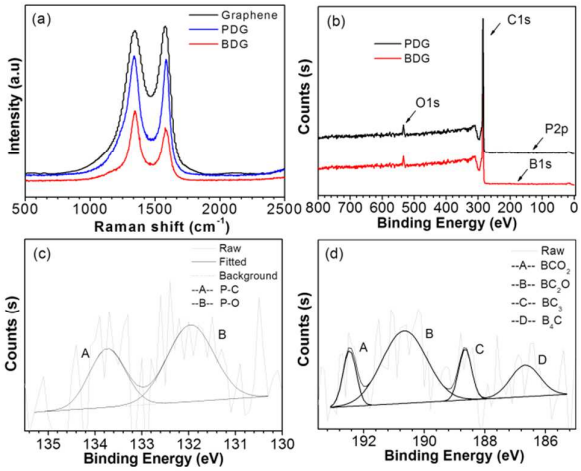

Fig. 3. (a) Raman spectra of PDG, BDG and pristine graphene, (b) wide XPS spectra, and high resolution XPS spectra of (c) P2p of PDG and (d) B1s of BDG.

To confirm chemical bonding between B or P and carbon (B-C or P-C), high resolution XPS spectra were shown in Fig. 3c, d. In PDG, phosphorus 2p (P2p) peak is observed at a binding energy of 132.1 eV, which is positively shifted compared to a binding energy of pure P2p peak (129.7 eV). Similarly, in BDG, boron 1s peak, observed at 189. 8 eV, is found to be positively shifted compared to binding energy of pure B1s peak (187 eV). These shifts of binding energies are ascribed to incorporated P or B into the graphene. After deconvolution of high resolution P2p spectrum, the P2p spectra on PDG are separated into two components, as shown in Fig.3c. For PDG, the highest binding energy at 133.7 eV is assigned to P-C bonding. The peak at 132.0 eV is due to P-O bonding. B1s peak of BDG catalyst is deconvoluted into four components as shown in Fig. 3d. The peak with the highest binding energy at 192.5 eV is derived from BCO_2. The peak observed at 190.7 eV is owing to BC_2O. The peaks centered at 188.7 eV and 186.7 eV correspond to BC_3 and B_4C, respectively. The surface analysis observed by XPS, combined with ICP-MS elemental analysis strongly suggest the possibility of selective doping depending on pyrolysis temperature, and easy tuning of types of heteroatom doped into carbon materials without any consideration regarding precursor and other synthetic conditions.

The electrocatalytic activity was evaluated by using cyclic voltammetry and linear sweep voltammetry. In Fig. 4, CV of untreated pristine graphene shows an unclear cathodic peak at 0.65 V vs. RHE with a peak current of 0.9 $mAcm^{-2}$. On the other hand, PDG and BDG exhibit a well-defined oxygen reduction cathodic peak at 0.66 V and 0.71 V vs. RHE with a peak current of 1.08 $mAcm^{-2}$ and 1.12 $mAcm^{-2}$. The observed current density value is about 1.1 times higher than that of the pristine graphene. In addition, the current density difference between the background and reduction curve at 0.7 V vs. RHE was compared among the prepared samples and the pristine graphene. The value of pristine graphene is found to be 0.47 $mAcm^{-2}$. However, the values of PDG and BDG are determined to be 0.67 $mAcm^{-2}$ and 1.1 $mAcm^{-2}$, and these are 1.4 to 2.4 times higher than that of the graphene. The above results indicate that heteroatom doping enhances the oxygen reduction current due to electronically modifying the pristine graphene by incorporating heteroatom into the graphene array. The most positive onset potential of the three samples is observed at 0.83 V vs. RHE for BDG sample. This value of BDG is 40 mV more positive than that of the untreated graphene.

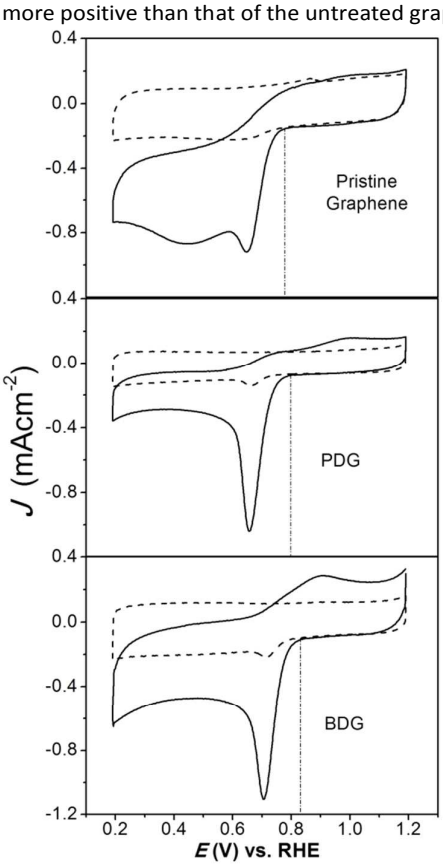

Fig. 4. Cyclic voltammograms of PDG, BDG, and pristine graphene. Dotted line for N_2-saturated 0.1 M KOH and solid line for O_2-saturated 0.1 M KOH.

This observation indicates that BDG enhances the oxygen reduction kinetics of the graphene better than PDG. In turn, this finding indicates that boron doping in graphene results in faster kinetics of the ORR with high current density. The evidence for this difference of the contribution between PDG

and BDG will be introduced in a latter section of the paper with hydrodynamic LSVs using RDE technique.

Figs. 5(a) and (b) depict LSVs and the insets corresponding Koutecky-Levich plots (K-L) of PDG and BDG. In LSVs, current density increases with an increase of the electrode rotation speed from 400 rpm to 2500 rpm, which follows Levich equation. At lower rotations, the LSVs show a peak around 0.67 V, which is due to the oxygen reduction and the reactant is depleted in the inner region and pores of the catalyst layer. This peak is disappeared at higher electrode rotations (>1600 rpm). The corresponding K-L plots show great linearity and good parallelism. The linearity and parallelism of the plots indicates first-order kinetics and constant electron transfer over a wide potential range.[32] In particular, all K-L plots of both prepared samples are found to have similar slope to ideal K-L plots when electron transfer is four, which suggest that both prepared samples follow four-electron pathway for oxygen reduction. ORR performance was enhanced by increasing the pyrolysis temperature from 700 °C to 900 °C.

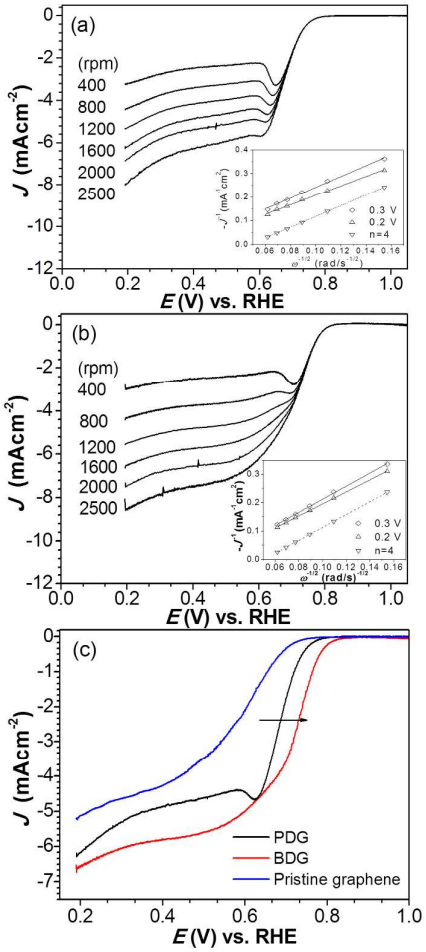

Fig. 5. Hydrodynamic linear sweep voltammograms (LSVs) of the ORR on (a) PDG, and (b) BDG in 0.1 M KOH at 10 mVs^{-1} at various electrode rotation speeds. Inset: corresponding K-L plots, (c) LSVs of the ORR on PDG, BDG, and Pt/C in 0.1 M KOH at 10 mVs^{-1} at 1600 rpm.

Fig. 5(c) compares the ORR activities of PDG, BDG and pristine graphene catalysts at the electrode rotation speed of 1600 rpm. The calculated *n* values of PDG and BDG are 3.98 and 3.94, while the values for pristine graphene are 2.1 to 2.7, as reported by Sheng et al.[28] These results suggest that heteroatom (B or P) doping into the graphene has the possibility to induce single-step four-electron transferred oxygen reduction like Pt-based catalysts. The onset potentials of PDG, BDG, and graphene are found to be 0.80, 0.83, and 0.79 V, which is similar to the values observed in CVs. The BDG catalyst showed 30 mV positive shift of the onset potential compared with the PDG (Table S1, Supporting Information). The half-wave ($E_{1/2}$) potentials of PDG, BDG and pristine graphene was found to be 0.68, 0.72, and 0.55 V, respectively. The $E_{1/2}$ of BDG catalyst is 40 mV more positive than a PDG catalyst and 170 mV higher than pristine graphene catalyst (Fig.5c). In comparing PDG and BDG catalysts, BDG shows higher oxygen reduction performance than a PDG. This difference is ascribed to differences of defect concentration related to sp^3 disordered carbon between the two samples owing to different doping level (Table S1, Supporting Information). The doping concentrations of PDG and BDG are different although synthetic precursor that possesses simultaneously P and B with same atomic concentration was used for pyrolysis. The higher doping concentration of BDG results from much easier doping of boron due to the similar covalent radius of boron with carbon atom rather than the doping of phosphorous into the carbon network. As mentioned previously, the difference of doping level induced more defect sites in samples that can act as harsh reaction sites. Namely, the presence of more reaction sites for ORR in BDG contributed to the higher electrocatalytic activity of the ORR.

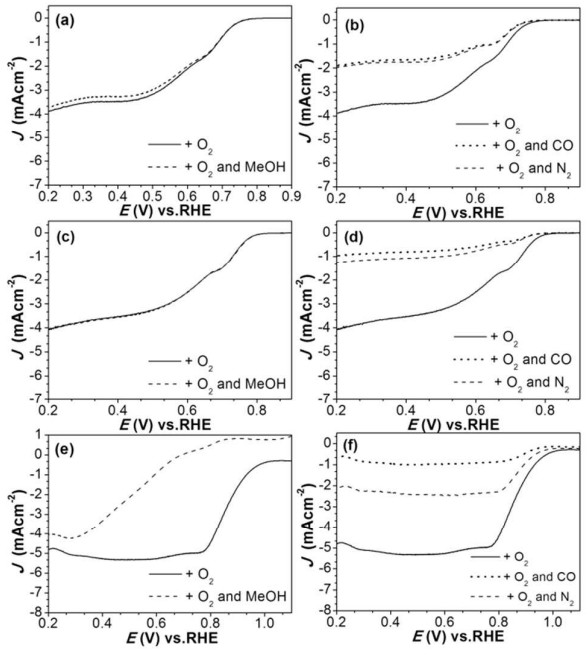

Fig. 6. LSVs with addition of 2 M methanol on (a) PDG, (c) BDG, and (e) Pt/C. LSVs with addition of CO (blue line) and N_2 gases (red line) at the same flow rate as O_2 gas on (b) PDG, (d) BDG, and (f) Pt/C in O_2-saturated 0.1 M KOH solution at 1600 rpm.

Figs. 6(a), (c), and (e), depict the selectivity studies of PDG, BDG, and commercial Pt/C catalysts for ORR in the presence methanol fuel. The solid line was obtained in O_2-saturated electrolyte, and the dotted line was obtained in methanol added O_2-saturated electrolyte. The solid and the dotted lines in LSVs of PDG and BDG closely overlap; however, the dotted line in LSV of Pt/C is not matched significantly and forms a gap with the solid line. This gap observed in LSVs of Pt/C corresponds to the oxygen reduction current decay due to simultaneous methanol oxidation, and strongly suggests the outstanding methanol tolerance of PDG and BDG. The results of CO poisoning effect test on the oxygen reduction are illustrated in Fig. 6(b), (d) and (f) for PDG, BDG, and Pt/C, respectively. The solid line was attained in O_2-saturated electrolyte, and the dotted blue line was obtained in both CO and O_2-saturated electrolyte. To consider a decrease in O_2 partial pressure owing to the addition of CO gases, the dotted red line was obtained in both N_2- and O_2-saturated electrolyte. For PDG and BDG catalysts, the dotted blue line and the dotted red line are closely matched. On the other hand, the blue line and the red line in LSV of Pt/C show critical disparity. This disparity suggests that the oxygen reduction on commercial Pt/C electrode can affected by CO poisoning while PDG and BDG show strong resistance against CO poisoning.

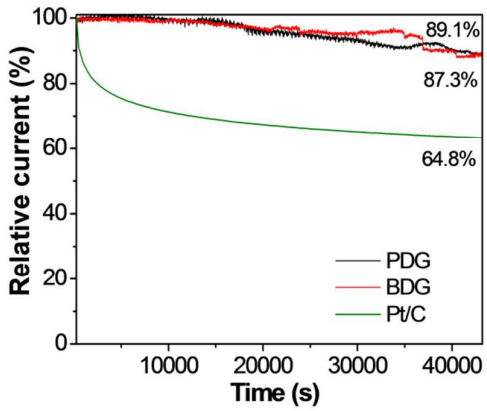

Fig. 7. Chronoamperometric response of PDG, BDG, and Pt/C at -0.26 V vs. SCE in O_2-saturated 0.1 M KOH solution for durability test during 12 h.

The electrochemical ORR stability of metal-free heteroatom-doped graphene catalysts were evaluated by chronoampherometric technique for a period of 12 h. Fig. 7 indicated the relative current decay of Pt/C electrode to 64.8%. On the contrary, PDG and BDG catalysts exhibit better durability than a Pt/C catalyst. The relative current decay of PDG and BDG catalysts was found to be 87% and 89%, respectively, suggesting that these both PDG and BDG catalysts exhibit long-term stability in ORR in alkaline medium.

4. Conclusion

A facile solid-state pyrolysis route was introduced to fabricate heteroatom-doped graphene as a non-precious catalyst for oxygen reduction. The elemental analysis reveals a selective doping of either phosphorous or boron was observed by tuning of pyrolysis temperature. The BDG catalyst exhibited improved oxygen reduction activity than PDG catalyst in an alkaline medium and enhanced electrocatalytic activity of BDG electrode was derived from more defects site on the catalyst than PDG due to difference of doping level. The durability of PDG and BDG electrode was much better than the Pt/C. In addition, tolerance of methanol oxidation and CO poisoning of PDG and BDG was outstanding compared with the commercial Pt/C. These results strongly suggest that heteroatom doping and pyrolysis synthetic route can be a rational approach for non-precious and metal-free catalysts for oxygen reduction and various catalytic applications.

Acknowledgement

This work was supported by the grant from the DGIST R&D Program (15-BD-01) of the Ministry of Education, Science, and Technology of Korea. We thank Centre for Core Research Facilities (CCRF) in Daegu Gyeongbuk Institute of Science and Technology, Korea.

Notes and references

[a] Department of Energy Systems Engineering, Daegu Gyeongbuk Institute of Science and Technology (DGIST), Daegu, 711-873, Republic of Korea.
E-mail: sangarajus@dgist.ac.kr; Fax: (+82) 53 785 6409.
†Electronic Supplementary Information (ESI) available: additional results. See DOI: 10.1039/c000000x/

1 D. Papegeorgopoulos, US DOE Fuel Cell Technologies Program: An Introduction to the 2010 Fuel Cell Pre-Solicitation Workshop, US DOE Fuel Cell Technologies Program: Department of Energy, 2010.
2 J. R. Varcoe, R. C. T. Slade, and E. Lam How Yee, *Chem. Commun.*, 2006, 1428–1429.
3 Z. W. Liu, F. Peng, H. J. Wang, H. Yu, W. X. Zheng, and J. Yang, *Angew. Chemie Int. Ed.*, 2011, **50**, 3257–3261.
4 C. H. Choi, S. H. Park, and S. I. Woo, *ACS Nano*, 2012, **6**, 7084–7091.
5 H. Wang, T. Maiyalagan, and X. Wang, *ACS Catal.*, 2012, **2**, 781–794.
6 S. Shanmugam and T. Osaka, *Chem. Commun.*, 2011, **47**, 4463–4465.
7 L. Yang, S. Jiang, Y. Zhao, L. Zhu, S. Chen, X. Wang, Q. Wu, J. Ma, Y. Ma, and Z. Hu, *Angew. Chemie Int. Ed.*, 2011, **50**, 7132–7135.
8 G. Jo and S. Shanmugam, *Electrochem. Commun.*, 2012, **25**, 101–104.
9 M. Terrones, A. G. S. Filho, and A. M. Rao, in Carbon Nanotubes Vol. 111 Topics in Applied Physics Ch. 17, 531-566, Springer Berlin Heidelberg, 2008.
10 S. Cui, P. Scharff, C. Siegmund, D. Schneider, K. Risch, S. Klötzer, L. Spiess, H. Romanus, and J. Schawohl, *Carbon N. Y.*, 2004, **42**, 931–939.

11 P. Redlich, J. Loeffler, P. M. Ajayan, J. Bill, F. Aldinger, and M. Riihle, *Chem. Phys. Lett.*, 1996, **4**, 465–470.
12 M. Terrones, W. K. Hsu, S. Ramos, R. Castillo, and H. Terrones, *Fuller. Sci. Technol.*, 1998, **6**, 787–800.
13 Y. Zhang, H. Gu, K. Suenaga, and S. Iijima, *Chem. Phys. Lett.*, 1997, **279**, 264–269.
14 P. L. Gai, O. Stephan, K. McGuire, A. M. Rao, M. S. Dresselhaus, and G. Dresselhaus, *J. Mater. Chem.*, 2004, **14**, 669–675.
15 S. Kundu, T. C. Nagaiah, W. Xia, Y. Wang, S. Van Dommele, J. H. Bitter, M. Santa, G. Grundmeier, M. Bron, W. Schuhmann, and M. Muhler, *J. Phys. Chem. C*, 2009, **113**, 14302–14310.
16 G. Keskar, R. Rao, J. Luo, J. Hudson, J. Chen, and A. M. Rao, *Chem. Phys. Lett.*, 2005, **412**, 269–273.
17 M. Vikkisk, I. Kruusenberg, U. Joost, E. Shulga, I. Kink, and K. Tammeveski, *Appl. Catal. B Environ.*, 2014, **147**, 369–376.
18 M. Endo, T. Hayashi, S.-H. Hong, T. Enoki, and M. S. Dresselhaus, *J. Appl. Phys.*, 2001, **90**, 5670–5674.
19 M. R. Philpott and Y. Kawazoe, *J. Chem. Phys.*, 2012, **137**, 054715–054765.
20 T. Hagio, M. Nakamizo, and K. Kobayashi, *Carbon N. Y.*, 1989, **27**, 259–263.
21 X. Kong and Q. Chen, *J. Mater. Chem.*, 2012, **22**, 15336–15341.
22 M. Zhang and L. Dai, *Nano Energy*, 2012, **1**, 514–517.
23 L. Zhang and Z. Xia, *J. Phys. Chem. C*, 2011, **115**, 11170–11176.
24 K. Takai, M. Oga, H. Sato, T. Enoki, Y. Ohki, A. Taomoto, K. Suenaga, and S. Iijima, *Phys. Rev. B*, 2003, **67**, 1–11.
25 M. Endo, Y. a. Kim, T. Hayashi, K. Nishimura, T. Matusita, K. Miyashita, and M. S. Dresselhaus, *Carbon N. Y.*, 2001, **39**, 1287–1297.
26 D. G. Larrude, M. E. H. Maia Da Costa, F. H. Monteiro, a. L. Pinto, and F. L. Freire, *J. Appl. Phys.*, 2012, **111**.
27 Z.-H. Sheng, H.-L. Gao, W.-J. Bao, F.-B. Wang, and X.-H. Xia, *J. Mater. Chem.*, 2012, **22**, 390–395.
28 H. Liu, Y. Liu, and D. Zhu, *J. Mater. Chem.*, 2011, **21**, 3335–3345.
29 J. S. Burgess, C. K. Acharya, J. Lizarazo, N. Yancey, B. Flowers, G. Kwon, T. Klein, M. Weaver, A. M. Lane, C. Heath Turner, and S. Street, *Carbon N. Y.*, 2008, **46**, 1711–1717.
30 S. Baik and J. W. Lee, *RSC Adv.*, 2015, **5**, 24661–24669.
31 J. Tai, J. Hu, Z. Chen, and H. Lu, *RSC Adv.*, 2014, **4**, 61437–61443.
32 M. R. Miah and T. Ohsaka, *Electrochim. Acta*, 2009, **54**, 5871–5876.

Graphical Abstract

Phosphorous and boron-doped graphene prepared using a single precursor showed reasonable oxygen reduction activity and excellent stability in alkaline electrolyte.